ACS OMEGA

Open Access

http://pubs.acs.org/journal/acsodf

Article

A Molecular Dynamics Study on Xe/Kr Separation Mechanisms Using Crystal Growth Method

Liangliang Liu, Dawei Guan, Yi Lu,* Mingrui Sun, Yu Liu, Jiafei Zhao, and Lei Yang*

Cite This: *ACS Omega* 2024, 9, 25822−25831

Read Online

ACCESS | Metrics & More | Article Recommendations

ABSTRACT: The separation of xenon/krypton gas mixtures is a valuable but challenging endeavor in the gas industry due to their similar physical characteristics and closely sized molecules. To address this, we investigated the effectiveness of the hydrate-based gas separation method for mixed Xe−Kr gas via molecular dynamics (MD) simulations. The formation process of hydrates facilitates the encapsulation of guest molecules within hydrate cages, offering a potential strategy for gas separation. Higher temperatures and pressures are advantageous for accelerating the hydrate growth rate. The final occupancy of guest molecules and empty cages within 5^{12}, $5^{12}6^4$, and all hydrate cages were thoroughly examined. An increase in the pressure and temperature enhanced the occupancy rates of Xe in both 5^{12} and $5^{12}6^4$ cages, whereas elevated pressure alone improved the occupancy of Kr in $5^{12}6^4$ cages. However, the impact of temperature and pressure on Kr occupancy within 5^{12} cages was found to be minimal. Elevated temperature and pressure resulted in a reduced occupancy of empty cages. Predominantly, $5^{12}6^4$ cages were occupied by Xe, whereas Kr showed a propensity to occupy the 5^{12} cages. With increasing simulated pressure, the final occupancy of Xe molecules in all cages rose from 0.37 to 0.41 for simulations at 260 K, while the final occupancy of empty cages decreased from 0.24 to 0.2.

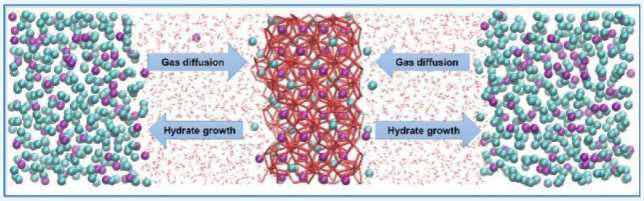

1. INTRODUCTION

Clathrate hydrates are crystalline substances that encapsulate molecules such as methane, CO_2, and N_2 within water molecule-formed polyhedral cages through hydrogen bonding under conditions of low temperature and high pressure. Common hydrates are classified into three dominant types, structures I, II, and H, which are influenced by the sizes of guest molecules.[1−3] Structure I (sI) hydrate has two pentagonal dodecahedral (5^{12}) cages and six tetrakaidecahedral ($5^{12}6^2$) cages, while structure II (sII) hydrate consists of 16 pentagonal dodecahedral (5^{12}) and eight hexakaidecahedral ($5^{12}6^4$) cages and can encapsulate larger molecules including C_3H_8. Structure H (sH) hydrate, on the contrary, is formed by three pentagonal dodecahedral (5^{12}) cages, two irregular dodecahedral ($4^35^66^3$) cages, and one icosahedral ($5^{12}6^8$) cage.[1,3]

Natural gas hydrates (NGHs) are emerging as promising alternative energy sources due to their abundant reserves,[4−7] containing twice the organic carbon compared to traditional fossil fuels.[8−15] Their applications extend beyond energy, playing roles in CO_2 capture,[16−18] flow assurance in oil/gas pipelines,[1,2,19,20] advancing separation technology,[21−23] etc. Specifically, they are highly efficient in gas mixture separations, highlighting their importance in gas separation processes.[24−29] Xenon (Xe) and Krypton (Kr), vital in industries such as nuclear, aerospace, lighting, medicine, and research,[30] share close physical properties and molecular sizes, making their separation challenging yet crucial for the gas industry.[31] Traditionally, Xe and Kr, two noble gases that are currently commercially available, are byproducts of the cryogenic distillation of air.[32] According to different working principles, cryogenic distillation, adsorption, membrane separation, and pressure swing adsorption have been proposed. However, these methods will result in high cost and low efficiency. Effective separation of rare gases is achieved by changing the pore size and surface modification properties of MOF materials, enabling gas separation in a mild environment.[33] Therefore, developing reliable techniques for separating mixed Xe/Kr is imperative, and a possible solution is hydrate-based gas separation. This method involves the continuous encapsulation of guest molecules during the growth of hydrates, which can enrich the target molecules in the hydrate phase under appropriate temperature and pressure conditions.

The study underscores the importance of identifying optimal conditions for the formation of gas hydrates to enhance the efficiency of separation and growth rates, particularly in the context of employing hydrate-based methods for mixed gas separation. Previous experiments have yielded critical data for

Received: January 4, 2024
Revised: March 31, 2024
Accepted: May 23, 2024
Published: June 4, 2024

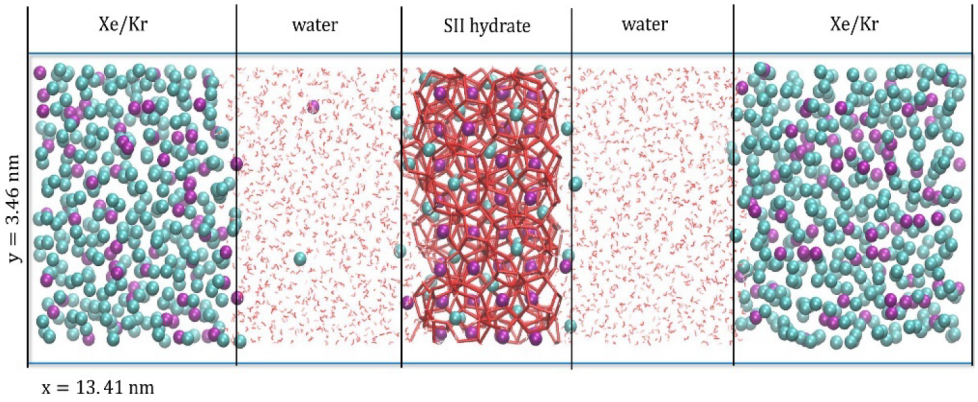

Figure 1. Typical initial configuration for mixed Xe/Kr hydrate growth. Cyan spheres: Xe in the gas phase or hydrate phase; blue spheres: Kr in the gas phase or hydrate phase; red sticks: hydrate seeds; and red lines: liquid water.

the application of such technologies in flue gas separation and storage, including information on phase equilibrium. Research by Handa et al. on the structural transformation in mixed hydrates of Xe and Kr based on gas composition, using NMR cross-polarization spectra, revealed a structural shift from sII to sI in the hydrate when the Xe concentration in the initial gas mix surpasses roughly 5 mol %. It was noted that the concentration of Xe in the gas phase at equilibrium with the hydrate is significantly lower than 5 mol %, indicating a pronounced enrichment of Xe within the hydrate phase.[34] Under pressures greater than 1.5 MPa (up to 1.7 GPa) at 273 K, pure Xe is known to form a stable sI hydrate.[35] However, at 263.61 K, the pressure requirements for maintaining the Xe hydrate phase dropped to 0.102 MPa.[36] Therefore, Xe can be captured in a clathrate hydrate at or below atmospheric pressure and 263 K. In the pressure range of 1.6−400 MPa and at temperatures close to the melting point of ice, pure Kr is known to form an sII hydrate.[37] Xe/Kr gas separation and identified Xe and Kr distributions in mixed clathrate hydrates synthesized from Xe/Kr vapor with various feed compositions have been studied.[38]

Exploring how mixed Xe/Kr hydrates develop under different temperatures and pressures presents a fascinating area of study, although uncovering the specifics can prove to be complex, especially when gas diffusion mechanisms are not easily understood. This complexity is due to the variety of forces at play that can influence the timing of hydrate formation, complicating efforts to maintain the stability of hydrates under conditions of minimal subcooling. MD simulations have been used to simulate hydrate processes for a long time to reveal nucleation theory,[39−45] hydrate dissociation processes,[46−50] hydrate conductivity,[51] etc. Míguez et al.[52] performed a three-phase coexistence simulation for CO_2 hydrate and obtained the melting temperatures at various pressures, which provided a fundamental technique to use MD simulations to obtain the phase equilibrium information. Similarly, Zhang et al.[53] performed simulations for the mixed hydrate growth process. They obtained the occupancy of pure Xe molecules in the hydrate cage and observed the different hydrate structure when guest molecule composition changed. Although previous studies have provided many explorations of the methods to obtain hydrate equilibrium data using MD simulations, most of them focus on the simulation of pure gas.[52,54−56] These works have made great contributions to the exploration of the molecular behaviors of gas hydrate growth.

In the study, molecular dynamics (MD) simulations were utilized to delve into the fundamental mechanisms behind the growth of Xe/Kr hydrates, starting with the initial sII hydrate seeds. The research aimed to understand the molecular diffusion process by observing the behavior of the mixed gases at various temperatures and pressures. Furthermore, the investigation covered the rate at which the hydrates grew and how the guest molecules occupied the hydrate structure, shedding light on the potential of Xe/Kr separation efficiency, given different driving forces.

2. METHODS

Molecular dynamics (MD) simulations were utilized to examine the effectiveness of separating Xe/Kr mixtures via the encapsulation process in the growth of sII hydrates. The study modeled a gas mixture with a composition reflective of industrial relevance comprising approximately 20% Kr and 80% Xe. The focus was on the dynamics of hydrate formation and the occupancy rates of the molecular cages. The initial configuration was created by setting a 2 × 2 × 2 unit cell replica of the sII hydrate with Xe/Kr molecules fully occupying all 5^{12} and $5^{12}6^4$ cages at the center (Xe occupy all $5^{12}6^4$ cages and Kr occupy all 5^{12} cages). This initial setup was surrounded by symmetrically distributed phases of water and Xe/Kr gas, with the gas phase containing 400 Xe molecules and 100 Kr molecules on each side, alongside 1358 liquid water molecules per side. The configuration is detailed in Figure 1. The system underwent a 1 ns NVT simulation at 270 K followed by a 3 ns NPT simulation under specific temperature and pressure conditions, utilizing a Berendsen barostat for system equilibration. After the preequilibrium process, formal NPT simulations were performed for hydrate growth and gas separation mechanisms.

The force field parameters are from the study conducted by Poling et al.[57] for Xe/Kr molecules, and Zhang et al.[58] have used this force field in hydrate growth research. TIP4P/ice[59] for water was used for all simulations. Water molecules were constrained to be rigid by employing the SHAKE/LINCS algorithm.[60,61] The simulations used a 2 fs time step using the leapfrog algorithm. The nonbonded interactions were calculated using Lennard−Jones potentials with a 1.0 nm cutoff distance for short-range interactions. The potential parameters for the cross-interactions of water, nitrogen, and carbon dioxide employed the Lorentz−Berthelot mixing rules. Long-range electrostatic interactions were calculated using the smooth particle mesh Ewald summation algorithm.[62] The

https://doi.org/10.1021/acsomega.4c00108
ACS Omega 2024, 9, 25822−25831

temperature was controlled using the Nosé−Hoover thermostat at formal simulations (after preequilibrium process),[63] and the pressure was controlled using the Parrinello−Rahman barostat[64] with damping constants of 4 and 10 ps, respectively. All simulations were performed using Gromacs 2019.4.[65,66] Periodic boundary conditions were imposed in all directions. Visual analyses for the trajectories were performed using VMD,[67] and nonvisual analyses were performed using custom codes developed in Python. Three independent simulations were performed for each system to obtain the average results.

3. RESULTS AND DISCUSSION

MD simulations have emerged as a critical approach for investigating the fundamental processes of gas hydrate formation, including nucleation[41,42,68−71] and growth,[23,72−74] at a molecular level. While much of the research has concentrated on the properties of pure gas hydrates, there is a growing body of work aimed at understanding the growth mechanisms of these hydrates, especially near their melting points.[52,54,55,75] This research lays the groundwork for employing direct phase coexistence methods to explore the development of mixed gas hydrates. Our study initially focused on the basic growth patterns of hydrates in the presence of preexisting sII hydrate seeds. We then examined the growth rates under a variety of simulation conditions, leading to an analysis of cage occupancy and the selectivity of these cages toward different gases.

3.1. Hydrate Growth and Molecular Diffusion. The development of mixed gas hydrates is significantly influenced by the specific conditions of growth, such as temperature and pressure, which can alter both the rate at which hydrates form and the inclusion rates of guest molecules, affecting phase equilibrium in the process. To investigate the patterns in which mixed gas hydrates grow, simulations were conducted at varying pressures (100, 300, and 500 bar) and temperatures (260, 270, and 280 K) to analyze both the rate of hydrate formation and the final occupancy rates of the guest molecules. Figure 2 illustrates the hydrate formation at conditions of 500 bar and 260 K. Initially, the liquid water did not contain any dissolved Xe or Kr molecules, leading to a diffusion process over 20 ns, where guest molecules moved from the gas to the liquid phase, supplying the necessary gas for the growth of hydrates. Thereafter, hydrate cages grew in front of the hydrate seeds (Figure 2a,b). As guest molecules from both the gas and hydrate phases diffuse into liquid water, the guest molecule concentration surpasses the equilibrium value. Subsequently, the hydrate growth process is initiated and continues until almost all liquid water molecules are consumed. As reported in previous studies,[55,72] during hydrate growth, water molecules located at the interface between the hydrate and water layer are consumptively prioritized, resulting in newly formed cages regularly appearing parallel to the hydrate/water interface (Figure 2b,c). Ultimately, as the hydrate growth process approaches completion, the hydrate growing edge reaches the gas phase, prompting continuous decomposition and reconstruction of hydrate cages located at the hydrate−gas interface to facilitate guest molecule exchange between the cages at the interface and the gas phase (Figure 2d).

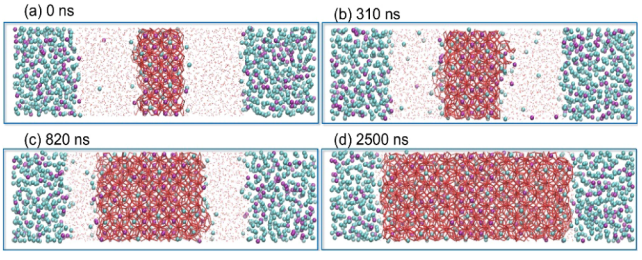

Figure 2. Snapshots of the growth process of mixed Xe/Kr gas hydrate at 500 bar and 260 K. (a−b) Guest molecules diffuse into liquid water and hydrate cages grow in front of hydrate seeds; (c−d) hydrate structure grows stably until nearly all liquid water is consumed.

To evaluate the process of crystal growth, the study utilized both the four-body order parameter (F_4)[43] and the changes in potential energy to monitor the onset of hydrate formation. Figure 3 depicts the progression of both the potential energy and the F4 order parameter as indicators of hydrate growth. The F_4 parameter can be defined as follows:

$$F_4 = \langle \cos 3\theta \rangle \quad (1)$$

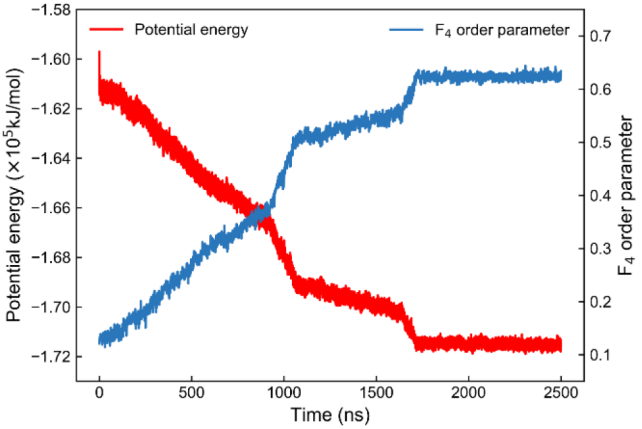

Figure 3. Evolution of potential energy and F_4 order parameter to quantify hydrate growth process for the simulation at 500 bar and 260 K. Red line: potential energy; blue line: F_4 order parameter.

Where θ is the torsion angle of the configuration H−O···O−H formed with the outmost hydrogen atoms of two adjacent water molecules.[43] For hydrate, liquid water, and ice, the values of F_4 are 0.7, −0.04, and −0.4, respectively.[43] During the first 5 ns, the gas phase was compressed to stable condition, and the value of potential energy decreased sharply from -1.57×10^5 to -1.61×10^5 kJ/mol. The experiment begins with an initial higher F_4 order parameter (0.1) due to the presetting of sII hydrate seeds, differing from the typical value for liquid water (−0.04). After that, the hydrate grew stably for approximately 1740 ns. Meanwhile, the potential energy decreased to approximately -1.72×10^5 kJ/mol and then fluctuated around this number. Concurrently, the F_4 order parameter rises from 0.1 to 0.635, reflecting the orderly growth of the hydrate structure as it incorporates almost all the available liquid water. These results are in accordance with previous studies on hydrate nucleation and growth process.[23,58,76,77] However, the fluctuation of the value of potential energy and F_4 order parameter did not mean that the hydrate structure maintained stable. The hydrate growing edge reaches the gas phase, prompting continuous decomposition and reconstruction of hydrate cages located at the hydrate/gas interface to facilitate guest molecule exchange between the cages at the interface and

https://doi.org/10.1021/acsomega.4c00108
ACS Omega 2024, 9, 25822−25831

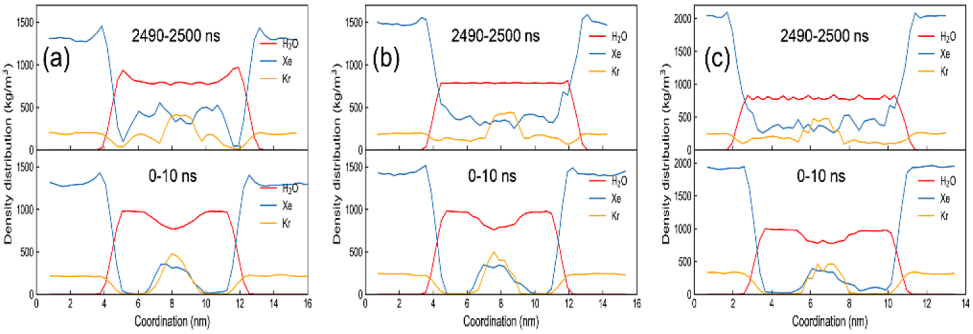

Figure 4. Density distribution functions in *x*-direction for the Xe/Kr hydrate growth process at 260 K. (a) Simulated results at 100 bar; (b) simulated results at 300 bar; and (c) simulated results at 500 bar.

the gas phase, which is in accordance with our observation from the snapshots in Figure 2.

Figure 4 depicts the density distribution functions in the *x*-direction for the Xe/Kr hydrate growth process at 260 K under different pressures (100, 300, and 500 bar). The upper and lower results in Figure 4 represent the average outcomes of the final 10 ns and initial 10 ns of simulations, respectively, displaying the growth behavior of the mixed gas hydrate. Higher pressure results in a shorter final box size, with the final box size in the *x*-direction measuring 15.414, 14.553, and 13.846 nm for simulated pressures of 100, 300, and 500 bar, respectively. Figure 4a shows the simulated pressure and temperature outcomes at 100 bar and 260 K, with Xe density in the gas phase weighing up to 1370 kg/m^3 (0−4 ns and 12−15.4 nm in the *x*-direction). With pressure increases to 300 and 500 bar, the Xe density in the gas phase also increases to 1760 kg/m^3 and 2130 kg/m^3 (Figure 4b,c), respectively. Similar density changes were observed for Kr in the gas phase. The hydrate growth process requires the common interaction of water and guest molecules.[78,79] To assess the crystal growth process, the researchers selected the four-body order parameter (F_4).[32] Greater guest molecule concentration typically results in more favorable hydrate growth (higher growth rate), as elaborated on in subsequent sections. In the liquid water region (4−6 nm and 10−12 nm), the average density values for Xe and Kr in Figure 4a were 45 kg/m^3 and 18 kg/m^3, respectively. Higher pressure also corresponded to higher density values of Xe and Kr in this region. At a pressure of 300 bar, the density values for Xe and Kr in liquid water rose to 71 kg/m^3 and 28 kg/m^3, respectively. Comparable density increments were observed as the pressure was increased to 500 bar. The findings suggested that higher pressure favored the molecular diffusion process, consistent with our previous investigations.[77] Additionally, the density distribution functions also can reflect spatial structure change for liquid water changed to the crystal structure. The density value in the liquid region (5−6 and 10−11 nm) decreased from 997.5 kg/m^3 during the initial 10 ns to 893 kg/m^3 for the last 10 ns, which indicated nearly all liquid water molecules were transmitted to the crystal structure.

3.2. Growth Rate Influenced by Pressure and Temperature. In the last section, we outlined the fundamental growth behaviors of Xe/Kr hydrate and utilized the F_4 order parameter to measure the hydrate growth process. External factors play a critical role in regulating the growth rate of hydrates, which is crucial for industrial applications. Consequently, we varied the pressure and temperature to investigate the mechanisms affecting the hydrate growth rate.

Figure 5 displays snapshots of the Xe/Kr hydrate growth process at 100 and 500 bar and 260 K. Figure 5a-d illustrates

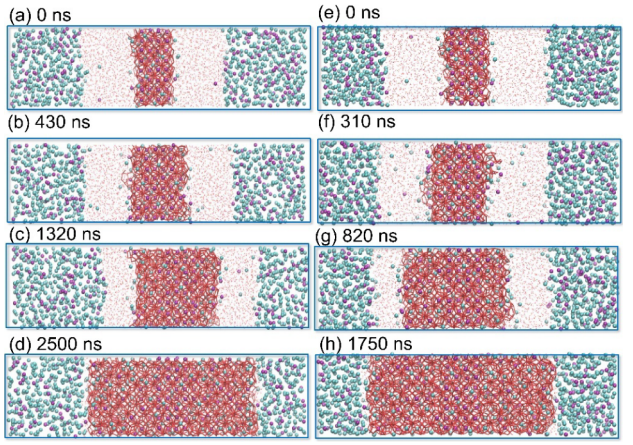

Figure 5. Snapshots of Xe/Kr hydrate growth process at 100 and 500 bar at 260 K. (a−d) Hydrate growth process at 100 bar and more residue liquid water were observed at the interface of hydrate front and gas phase; (e−h) hydrate growth process at 500 bar, and liquid water was almost consumed during the hydrate growth process.

the hydrate growth process at 100 bar, with successive hydrate growth observed. The overall simulation time revealed prior growth at the hydrate/water interface. A similar hydrate growth process was observed in simulations at a pressure of 500 bar (Figure 5e-h). Nonetheless, the simulation results at 100 bar displayed a lower hydrate growth rate and necessitated more simulation time for liquid water to become entirely crystalline. Additionally, the density distribution functions for water in Figure 4 indicate that the density value near the gas phase is close to that of liquid water and this is larger than the water density for the hydrate. This implies that more residual water was left in the system and weak molecular diffusion at lower pressure required more simulation time for hydrate growth.

As previously discussed in the last section, higher pressure can generate a greater driving force that favors improving the hydrate growth rate. Typically, a higher pressure facilitates increased guest molecule dissolution in water, which enhances the guest molecule solubility. At the same time, the guest molecules slowly diffuse into liquid water until they reach a stable value to sustain hydrate growth during the initial stage of hydrate growth.[80] To investigate the influence of pressure and temperature on the initial concentration of guest molecules in

https://doi.org/10.1021/acsomega.4c00108
ACS Omega 2024, 9, 25822−25831

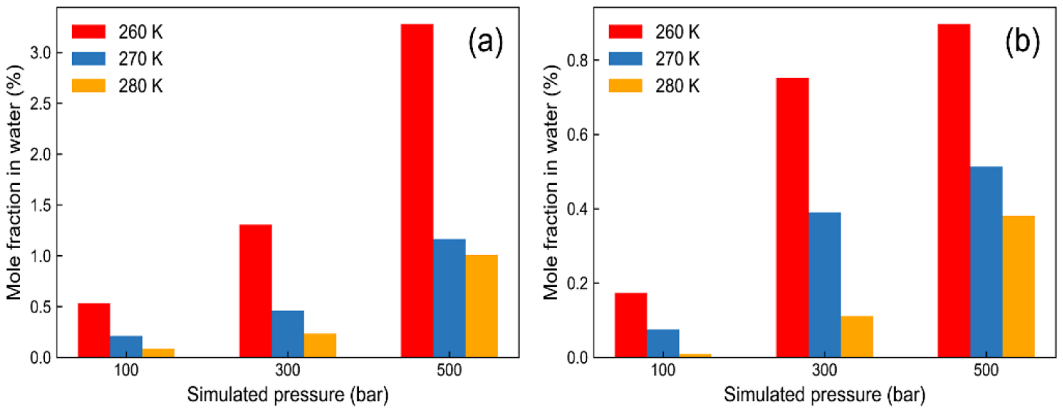

Figure 6. Equilibrium concentration of the guest molecules for simulations at 260 K. (a) Mole fraction of Xe; (b) mole fraction of Kr.

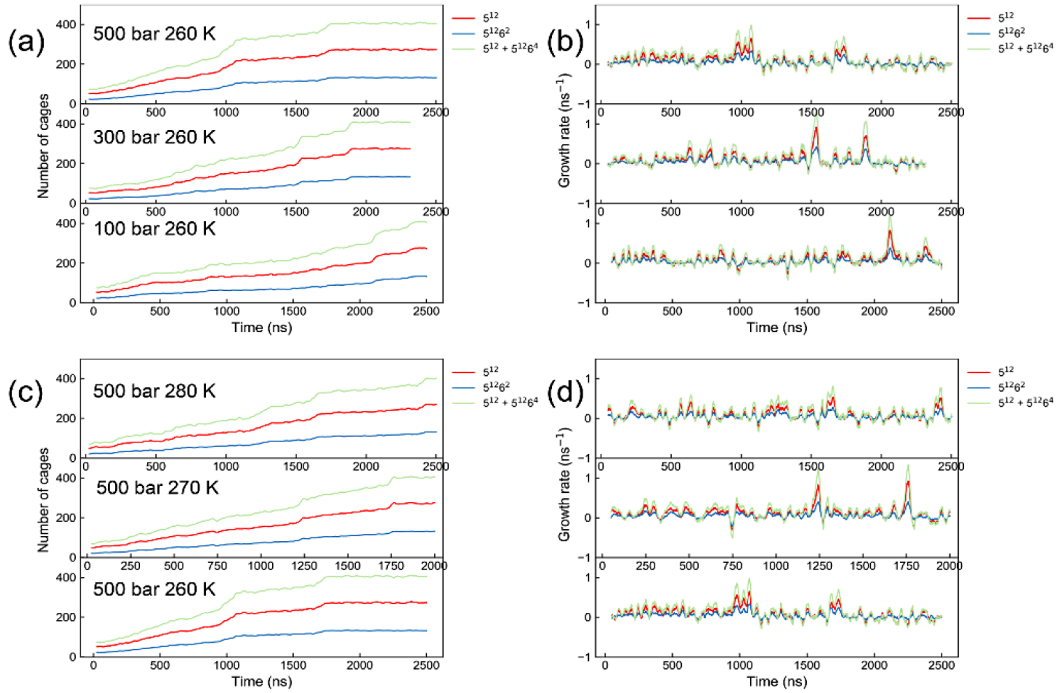

Figure 7. Evolution of the number of hydrate cage and growth rate at different pressure and temperature. (a) Cage number evolution at 260 K for different pressure; (b) growth rate at 260 K for different pressure; (c) cage number evolution at 500 bar for different temperatures; and (d) growth rate at 500 bar for different temperatures.

liquid water, the density distribution function data for water and Xe and Kr in Figure 4 was used to calculate the equilibrium concentration of guest molecules. Figure 6 shows the concentrations of Xe and Kr in liquid water using the average results of the first 10 ns of each simulation (after equilibrium). Figure 6a shows the simulated results for Xe. At 260 K, the mole fraction concentration of Xe molecules increased from 0.531% to 3.281% as the pressure increased from 100 to 500 bar. At 100 bar, the Xe concentration declined from 0.543% to 0.016% as the temperature increased from 260 to 280 K. Comparable outcomes were attained for Kr, but the value was lower because of its smaller molecular size compared to Xe.[38] Figure 6b displays the Kr results. At 260 K, the mole fraction concentration of Kr molecules rose from 0.174% to 0.897%, with pressure increasing from 100 to 500 bar. When the temperature increased from 260 to 280 K at 100 bar, the Xe concentration decreased from 0.174% to 0.009%.

In our simulation, the initial sII hydrate seeds provided a stable growing site for newly formed cages, which limited the newly formed crystal pattern to sII. This is in accordance with the results of the study conducted by Yi et al.[75] We created a code to determine hydrate cages and obtain the hydrate growth rate to measure the impact of pressure and temperature on the hydrate growth rate. Figure 7 illustrates the transition of the number of 5^{12}, $5^{12}6^4$, and all hydrate cages and the hydrate growth rate, defined as the change in hydrate cages per nanosecond. A positive value of the hydrate growth rate signifies hydrate growth, whereas a negative value denotes hydrate decomposition. Figure 7a,b exhibits the simulation results at 260 K, with the simulation time for liquid water to transform into a solid-like state decreasing from 2500 to 1700 ns as pressure increased. Furthermore, the hydrate growth rate corresponded with the cage evolution tendency. Compared with the 100-bar simulations, the improved pressure focused on the region with a positive value. In contrast, the hydrate

https://doi.org/10.1021/acsomega.4c00108
ACS Omega 2024, 9, 25822−25831

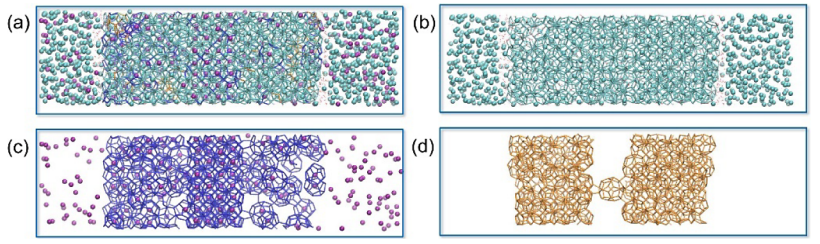

Figure 8. Snapshots of the final frame for the simulation at 260 K and 500 bar. (a) All hydrate cage and guest molecules;(b) hydrate cages occupied by Xe; (c) hydrate cages occupied by Kr; and (d) empty cages. Cyan sticks: hydrate cages occupied by Xe; blue sticks: hydrate cages occupied by Kr; and orange: empty cages.

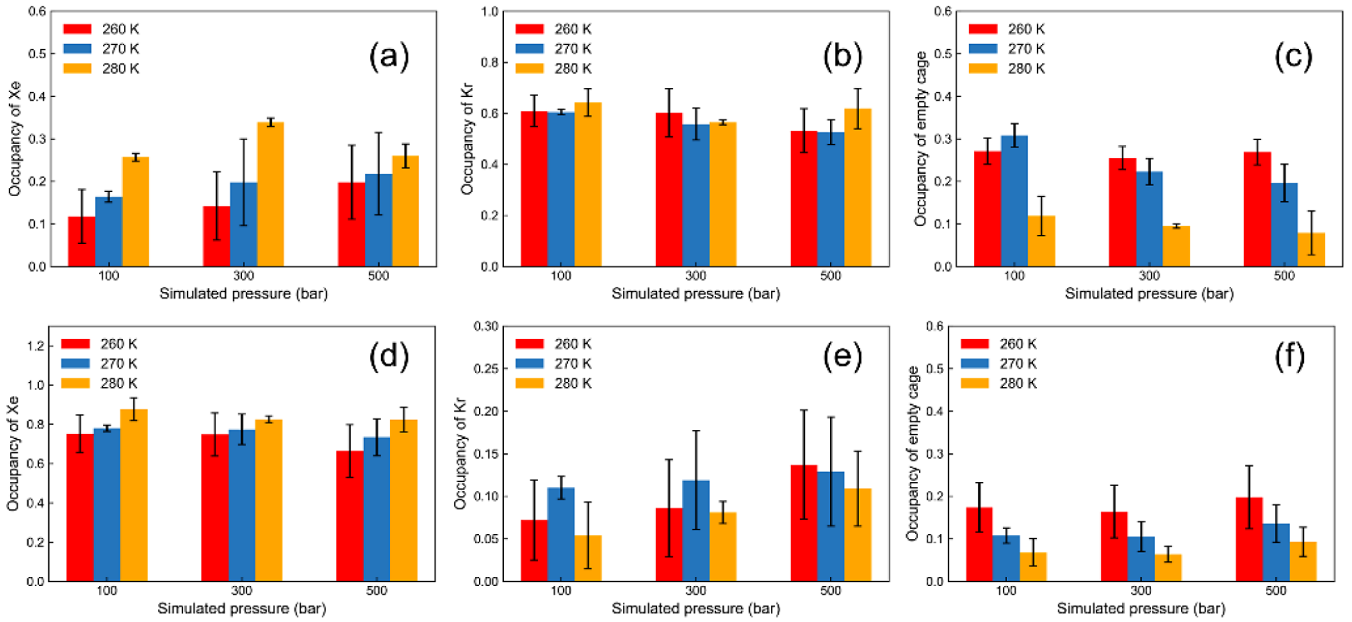

Figure 9. Results for the guest molecule selectivity analysis and occupancy between the 5^{12} and $5^{12}6^4$ cages at different pressure and temperatures for newly formed hydrate. Occupancy of (a) Xe in 5^{12} cages; (b) Kr in 5^{12} cages; (c) empty cages in 5^{12} cages; (d) Xe in $5^{12}6^4$ cages; (e) Kr in $5^{12}6^4$ cages; and (f) empty cages in $5^{12}6^4$ cages.

growth rate fluctuated around −0.2 to 0.9 ns^{-1} until the hydrate growth process was completed at 1700 ns for the simulation at 500 bar and 260 K. Figure 7c,d shows the simulation outcomes for different temperatures at 500 bar. The hydrate growth simulation times were prolonged due to smaller driving force (subcooling) compared to the simulation results at 260 K. This phenomenon verified that appropriate subcooling can reinforce the hydrate growth process.[81]

3.3. Cage Occupancy Analysis and Empty Cage. The hydrate growth process can encapsulate guest molecules in the cages. Different phase equilibrium conditions can result in different enrichment ratios, and proper pressure and temperature are key factors in efficiently separating mixed gas.[82] To investigate the separation efficiency of Xe/Kr mixed gas, the occupancy of guest molecules for the simulations were calculated. However, large quantities of empty cages were found when we analyzed the data. Figure 8 shows the snapshots of the final frame for the simulation at 260 K and 500 bar. The cyan sticks represented hydrate cages occupied by Xe, blue sticks represented hydrate cages occupied by Kr, and orange sticks represented empty cages. Figure 8a−c shows all hydrate cage and guest molecules, cages occupied by Xe, and cages occupied by Kr. Additionally, we show the empty cages in Figure 8d to make it clear. This phenomenon is in accordance with sII hydrate growth characteristics observed in the study conducted by Chen et al.[78] who studied propane hydrate nucleation and growth process and found empty cages were also important for this process.

The guest molecule selectivity analysis and occupancy between the 5^{12} and $5^{12}6^4$ cages at various pressures and temperatures of newly formed hydrate are presented in Figure 9. The results represent the average of the last 20 frames of three distinct simulations. Figure 9a−c displays the occupancy results of Xe, Kr, and empty cages in the newly formed 5^{12} hydrate cages in the system at different temperatures and pressures, eliminating the impact of the initial guest molecule configuration in the initial sII hydrate seeds. As the simulated pressure increases, the final occupancy of Xe molecules in 5^{12} cages increases from 0.12 to 0.21 for the simulations at 260 K; the same increasing tendency is also observed when the temperature was increased from 260 to 280 K, and the specific value of the occupancy for the simulations at 100 bar increases from 0.12 to 0.27. The study indicates that the occupancy of Kr in hydrate cages shows minimal sensitivity to variations in temperature and pressure, largely because Kr predominantly occupies the 5^{12} hydrate cages.[58] It was found that increasing temperature and pressure generally lead to a reduction in the number of empty cages, a result consistent with previous research.[77] Although a rise in temperature may decelerate the growth rate of hydrates, it positively affects the duration guest

https://doi.org/10.1021/acsomega.4c00108
ACS Omega 2024, 9, 25822−25831

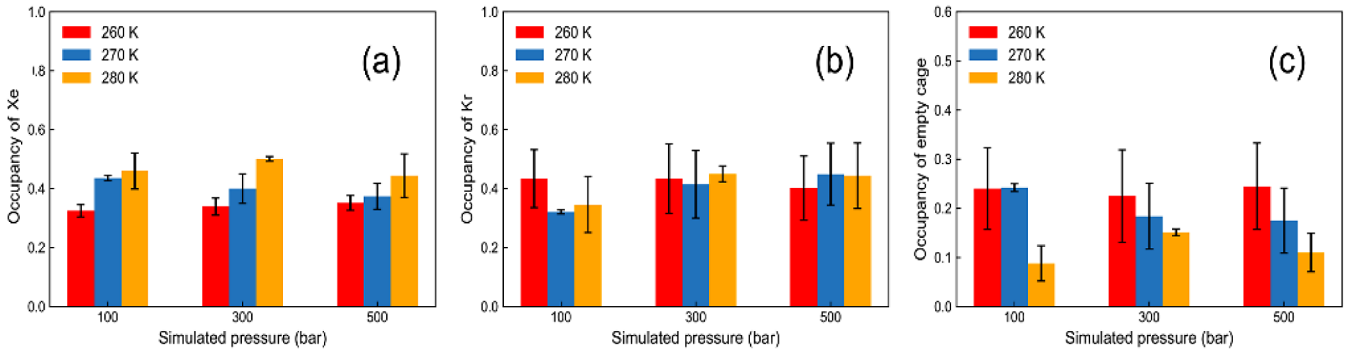

Figure 10. Results for the guest molecule occupancy for all cages at different pressures and temperatures for newly formed hydrate. Occupancy of (a) Xe in all cages; (b) Kr in all cages; and (c) empty cages in all cages.

molecules remain in the hydrate cages, contributing to the overall stability of the hydrate structure. Figure 9d–f displays the occupancy results of Xe, Kr, and empty cages in the newly formed $5^{12}6^4$ hydrate cages in the system at different temperatures and pressures. As the simulated pressure increases, the final occupancy of Xe molecules in $5^{12}6^4$ cages slightly decreases from 0.75 to 0.66 for the simulations at 260 K; However, the specific value of the Xe occupancy for the simulations at 100 bar increased from 0.75 to 0.88. The influence of temperature and pressure is weak for the occupancy of Xe, and this is because Xe tends to occupy $5^{12}6^4$ hydrate cages and occupy most of the $5^{12}6^4$ cages.[58] For Kr, a higher pressure improved its occupancy in $5^{12}6^4$ cages. In summary, higher pressure and temperature improved Xe occupancy both in 5^{12} and $5^{12}6^4$ cages; higher pressure improved Kr occupancy in $5^{12}6^4$ cages; however, the influence of temperature and pressure is weak for the occupancy of Kr in 5^{12} cages; higher temperature and pressure reduced the occupancy of empty cages.

Figure 10 shows the results for the guest molecule occupancy for all cages at different pressures and temperatures for newly formed hydrate. Figure 10a–c displays the occupancy results of Xe, Kr, and empty cages in the newly formed all hydrate cages in the system at different temperatures and pressures, eliminating the impact of the initial guest molecule configuration in the initial sII hydrate seeds. As the simulated pressure increases, the final occupancy of Xe molecules in all cages increases from 0.37 to 0.41 for the simulations at 260 K; the same increasing tendency is also observed when the temperature was increased from 260 to 280 K, and the specific value of the occupancy for the simulations at 100 bar increases from 0.37 to 0.45. However, the influence of temperature and pressure is weak for the occupancy of Kr. This is because Kr tends to occupy 5^{12} hydrate cages, and higher pressure and temperature also improved Xe occupancy in 5^{12} hydrate cages.[58] Higher temperature and pressure reduced the occupancy of empty cages, which is in accordance with our previous study.[77] Higher pressure improved the concentration of guest molecules, which is beneficial to the interaction of water and guest molecules to form hydrate cages.[78] Although mild temperature reduced hydrate growth rate, it assisted guest molecules to occupy hydrate cages for a longer time.

4. CONCLUSIONS

This study utilized MD simulations to explore the efficacy of the hydrate-based gas separation method for the Xe/Kr mixed gas. Different pressures (100, 300, and 500 bar) and temperatures (260, 270, and 280 K) were employed to analyze hydrate growth patterns and growth rates, and the following conclusions were reached.

(1) Hydrates are preferentially generated at the interface and grow in parallel to form new cages. Hydrate edges near the gas phase continue to disintegrate and rebuild.

(2) Higher temperatures and pressures favored accelerated hydrate growth rates and increased xenon occupancy in the 5^{12} and $5^{12}6^4$ cages.

(3) Higher pressures elevated the occupancy of krypton in the $5^{12}6^4$ cage but had less of an effect on krypton's occupancy in the 5^{12} cage.

(4) At increasing pressure, the final occupancy of xenon molecules in all cages increased from 0.37 to 0.41 at 260 K, while decreasing the occupancy of empty cages.

The hydrate method of separating xenon and krypton, which is achieved by the selectivity of the differences in the hydrate cage structure to monatomic gas molecules of different diameters, faces the following problems:

(1) The differences between the gas molecules are small; the improvement in purity is limited; and multiple separation cycles are required to achieve the desired level of purity.

(2) The separation efficiency of this method may not be as good as that of physical adsorption or cry-fractionation, especially when dealing with large gaseous mixtures.

And for the experiment itself:

(1) The hydrate method is relatively energy intensive with temperature stabilization maintained by external energy.

(2) The experimental operations are relatively complex, involving precise control of the temperature and pressure as well as stable formation and decomposition processes of hydrates.

Like other methods, the hydrate method has the potential for separating xenon and krypton. However, it faces a few challenges in terms of selectivity, separation efficiency, operating costs, and process control. Further research and development may be required to optimize the technology, reduce costs, and improve separation efficiency and purity before practical application.

AUTHOR INFORMATION

Corresponding Authors

Yi Lu − *Shenyang Aircraft Design Institute, Shenyang 110042, China*; Email: 2369636377@qq.com

Lei Yang − *Key Laboratory of Ocean Energy Utilization and Energy Conservation of Ministry of Education, Dalian*

https://doi.org/10.1021/acsomega.4c00108
ACS Omega 2024, 9, 25822−25831

University of Technology, Dalian 116024, China; orcid.org/0000-0003-1885-1789; Email: leiyang@dlut.edu.cn

Authors

Liangliang Liu − *Shenyang Aircraft Design Institute, Shenyang 110042, China*

Dawei Guan − *Key Laboratory of Ocean Energy Utilization and Energy Conservation of Ministry of Education, Dalian University of Technology, Dalian 116024, China;* orcid.org/0000-0001-6209-6755

Mingrui Sun − *Key Laboratory of Ocean Energy Utilization and Energy Conservation of Ministry of Education, Dalian University of Technology, Dalian 116024, China*

Yu Liu − *Key Laboratory of Ocean Energy Utilization and Energy Conservation of Ministry of Education, Dalian University of Technology, Dalian 116024, China;* orcid.org/0000-0002-6003-9121

Jiafei Zhao − *Key Laboratory of Ocean Energy Utilization and Energy Conservation of Ministry of Education, Dalian University of Technology, Dalian 116024, China;* orcid.org/0000-0001-8401-4204

Complete contact information is available at: https://pubs.acs.org/10.1021/acsomega.4c00108

Author Contributions

L.L. performed MD simulations and analyzed the data. Y. L., L.Y., and J.Z. provided suggestions and instructions. D.G., M.S., and Y. L. provided investigation and resources.

Notes

The authors declare no competing financial interest.

■ ACKNOWLEDGMENTS

This work was supported by the National Natural Science Foundation of China (Grant No. 52176002), the National Key R&D Program of China (Grant No. 2021YFC2800902), and the Dalian High-Level Talent Innovation Program (grant no. 2022RY06).

■ REFERENCES

(1) Sloan Jr, E. D.; Koh, C. A. *Clathrate hydrates of natural gases*; CRC Press: Boca Rator-L.-N, CRC press, 2008.

(2) Sloan, E. D. Fundamental principles and applications of natural gas hydrates. *Nature* **2003**, *426* (6964), 353−359.

(3) Koh, C. A. Towards a fundamental understanding of natural gas hydrates. *Chem. Soc. Rev.* **2002**, *31* (3), 157−167.

(4) Yang, L.; Shi, K.; Qu, A.; Liang, H.; Li, Q.; Lv, X.; Leng, S.; Liu, Y.; Zhang, L.; Liu, Y.; et al. The locally varying thermodynamic driving force dominates the gas production efficiency from natural gas hydrate-bearing marine sediments. *Energy* **2023**, *276*, 127545.

(5) Guan, D.; Qu, A.; Wang, Z.; Lv, X.; Li, Q.; Leng, S.; Xiao, B.; Zhang, L.; Zhao, J.; Yang, L.; et al. Fluid flow-induced fine particle migration and its effects on gas and water production behavior from gas hydrate reservoir. *Appl. Energy* **2023**, *331*, 120327.

(6) Li, Y.-L.; Ning, F.-L.; Xu, M.; Qi, M.-H.; Sun, J.-X.; Nouri, A.; Gao, D.-L.; Wu, N.-Y. Experimental study on solid particle migration and production behaviors during marine natural gas hydrate dissociation by depressurization. *Pet. Sci.* **2023**, *20* (6), 3610−3623.

(7) Li, Y.; Wang, L.; Xie, Y.; Wu, P.; Liu, T.; Huang, L.; Zhang, S.; Song, Y. Deformation characteristics of methane hydrate-bearing clayey and sandy sediments during depressurization dissociation. *Energy* **2023**, *275*, 127527.

(8) Guo, X.; Xu, L.; Wang, B.; Sun, L.; Liu, Y.; Wei, R.; Yang, L.; Zhao, J. Optimized gas and water production from water-saturated hydrate-bearing sediment through step-wise depressurization combined with thermal stimulation. *Appl. Energy* **2020**, *276*, 115438.

(9) Zhao, J.; Liu, Y.; Guo, X.; Wei, R.; Yu, T.; Xu, L.; Sun, L.; Yang, L. Gas production behavior from hydrate-bearing fine natural sediments through optimized step-wise depressurization. *Appl. Energy* **2020**, *260*, 114275.

(10) Boswell, R.; Collett, T. S. Current perspectives on gas hydrate resources. *Energy Environ. Sci.* **2011**, *4* (4), 1206−1215.

(11) Wallmann, K.; Pinero, E.; Burwicz, E.; Haeckel, M.; Hensen, C.; Dale, A.; Ruepke, L. The global inventory of methane hydrate in marine sediments: A theoretical approach. *Energies* **2012**, *5* (7), 2449−2498.

(12) Zhao, J.; Liu, Y.; Yang, L.; Zhang, L.; Song, Y. Organics-Coated Nanoclays Further Promote Hydrate Formation Kinetics. *J. Phys. Chem. Lett.* **2021**, *12* (13), 3464−3467.

(13) Hassanpouryouzband, A.; Yang, J.; Tohidi, B.; Chuvilin, E.; Istomin, V.; Bukhanov, B.; Cheremisin, A. Insights into CO2 Capture by Flue Gas Hydrate Formation: Gas Composition Evolution in Systems Containing Gas Hydrates and Gas Mixtures at Stable Pressures. *ACS Sustainable Chem. Eng.* **2018**, *6* (5), 5732−5736.

(14) Yang, L.; Falenty, A.; Chaouachi, M.; Haberthür, D.; Kuhs, W. F. Synchrotron X-ray computed microtomography study on gas hydrate decomposition in a sedimentary matrix. *Geochem., Geophys., Geosyst.* **2016**, *17* (9), 3717−3732.

(15) Wei, R.; Xia, Y.; Wang, Z.; Li, Q.; Lv, X.; Leng, S.; Zhang, L.; Zhang, Y.; Xiao, B.; Yang, S.; et al. Long-term numerical simulation of a joint production of gas hydrate and underlying shallow gas through dual horizontal wells in the South China Sea. *Appl. Energy* **2022**, *320*, 119235.

(16) Hassanpouryouzband, A.; Yang, J.; Tohidi, B.; Chuvilin, E.; Istomin, V.; Bukhanov, B. Geological CO2 Capture and Storage with Flue Gas Hydrate Formation in Frozen and Unfrozen Sediments: Method Development, Real Time-Scale Kinetic Characteristics, Efficiency, and Clathrate Structural Transition. *ACS Sustainable Chem. Eng.* **2019**, *7* (5), 5338−5345.

(17) Liu, Y.; Zhang, L.; Yang, L.; Dong, H.; Zhao, J.; Song, Y. Behaviors of CO2 Hydrate Formation in the Presence of Acid-Dissolvable Organic Matters. *Environ. Sci. Technol.* **2021**, *55* (9), 6206−6213.

(18) Yang, L.; Guan, D.; Qu, A.; Li, Q.; Ge, Y.; Liang, H.; Dong, H.; Leng, S.; Liu, Y.; Zhang, L.; et al. Thermotactic habit of gas hydrate growth enables a fast transformation of melting ice. *Appl. Energy* **2023**, *331*, 120372.

(19) Li, Y.; Wu, N.; Ning, F.; Gao, D.; Hao, X.; Chen, Q.; Liu, C.; Sun, J. Hydrate-induced clogging of sand-control screen and its implication on hydrate production operation. *Energy* **2020**, *206*, 118030.

(20) Chen, B.; Sun, H.; Li, K.; Yu, T.; Jiang, L.; Yang, M.; Song, Y. Unsaturated water flow-induced the structure variation of gas hydrate reservoir and its effect on fluid migration and gas production. *Energy* **2023**, *282*, 128843.

(21) Vorotyntsev, V. M.; Malyshev, V. M.; Mochalov, G. M.; Taraburov, P. G. Separation of gas mixtures by the gas hydrate crystallization method. *Theor. Found. Chem. Eng.* **2001**, *35* (2), 119−123.

(22) Lee, E. K.; Lee, J. D.; Lee, H. J.; Lee, B. R.; Lee, Y. S.; Kim, S. M.; Park, H. O.; Kim, Y. S.; Park, Y.-D.; Do Kim, Y. Pure SF 6 and SF 6 −N 2 Mixture Gas Hydrates Equilibrium and Kinetic Characteristics. *Environ. Sci. Technol.* **2009**, *43* (20), 7723−7727.

(23) Lu, Y.; Sun, L.; Guan, D.; Yang, L.; Zhang, L.; Song, Y.; Zhao, J. Molecular behavior of CO2 hydrate growth in the presence of dissolvable ionic organics. *Chem. Eng. J.* **2022**, *428*, 131176.

(24) Khatib, H. IEA world energy outlook 2011—A comment. *Energy Policy* **2012**, *48*, 737−743.

(25) Yang, M.; Zhou, H.; Wang, P.; Song, Y. Effects of additives on continuous hydrate-based flue gas separation. *Appl. Energy* **2018**, *221*, 374−385.

(26) Zhang, Q.; Zheng, J.; Zhang, B.; Linga, P. Coal mine gas separation of methane via clathrate hydrate process aided by tetrahydrofuran and amino acids. *Appl. Energy* **2021**, *287*, 116576.
(27) Ko, G.; Lee, J.; Seo, Y. Separation efficiency and equilibrium recovery ratio of SF6 in hydrate-based greenhouse gas separation. *Chem. Eng. J.* **2021**, *405*, 126956.
(28) Tang, J.; Zeng, D.; Wang, C.; Chen, Y.; He, L.; Cai, N. Study on the influence of SDS and THF on hydrate-based gas separation performance. *Chem. Eng. Res. Des.* **2013**, *91* (9), 1777−1782.
(29) Eslamimanesh, A.; Mohammadi, A. H.; Richon, D.; Naidoo, P.; Ramjugernath, D. Application of gas hydrate formation in separation processes: A review of experimental studies. *J. Chem. Thermodyn.* **2012**, *46*, 62−71.
(30) Lane, G. A.; Nahrwold, M. L.; Tait, A. R.; Taylor-Busch, M.; Cohen, P. J.; Beaudoin, A. R. Anesthetics as teratogens: nitrous oxide is fetotoxic, xenon is not. *Science* **1980**, *210* (4472), 899−901.
(31) Gong, L.; Ye, Y.; Liu, Y.; Li, Y.; Bao, Z.; Xiang, S.; Zhang, Z.; Chen, B. A microporous hydrogen-bonded organic framework for efficient Xe/Kr separation. *ACS Appl. Mater. Interfaces* **2022**, *14* (17), 19623−19628.
(32) Li, J.-R.; Kuppler, R. J.; Zhou, H.-C. Selective gas adsorption and separation in metal−organic frameworks. *Chem. Soc. Rev.* **2009**, *38* (5), 1477−1504.
(33) Li, L.; Guo, L.; Zhang, Z.; Yang, Q.; Yang, Y.; Bao, Z.; Ren, Q.; Li, J. A Robust Squarate-Based Metal−Organic Framework Demonstrates Record-High Affinity and Selectivity for Xenon over Krypton. *J. Am. Chem. Soc.* **2019**, *141* (23), 9358−9364.
(34) Handa, Y.; Ratcliffe, C.; Ripmeester, J.; Tse, J. Structural transition in mixed hydrates of xenon and krypton as a function of gas composition. *J. Phys. Chem.* **1990**, *94* (10), 4363−4365.
(35) Alavi, S.; Ripmeester, J. A. *Clathrate Hydrates: molecular Science and Characterization*; John Wiley & Sons, 2022.
(36) Rasoolzadeh, A.; Aaldijk, L.; Raeissi, S.; Shariati, A.; Peters, C. J. Experimental investigation and thermodynamic modeling of xenon clathrate hydrate stability conditions. *Fluid Phase Equilib.* **2020**, *512*, 112528.
(37) Dyadin, Y. A.; Larionov, E. G.; Mikina, T. V.; Starostina, L. I. Clathrate formation in Kr-H 2 O and Xe-H 2 O systems under pressures up to 15 kbar. *Mendeleev Commun.* **1997**, *7* (2), 74−76.
(38) Chu, H.; Shin, K. Highly-selective xenon−krypton separation using hydrate-based technology. *Sep. Purif. Technol.* **2023**, *319*, 124094.
(39) Barnes, B. C.; Knott, B. C.; Beckham, G. T.; Wu, D. T.; Sum, A. K. Reaction Coordinate of Incipient Methane Clathrate Hydrate Nucleation. *J. Phys. Chem. B* **2014**, *118* (46), 13236−13243.
(40) Barnes, B. C.; Beckham, G. T.; Wu, D. T.; Sum, A. K. Two-component order parameter for quantifying clathrate hydrate nucleation and growth. *J. Chem. Phys.* **2014**, *140* (16), 164506.
(41) Jacobson, L. C.; Molinero, V. Can Amorphous Nuclei Grow Crystalline Clathrates? The Size and Crystallinity of Critical Clathrate Nuclei. *J. Am. Chem. Soc.* **2011**, *133* (16), 6458−6463.
(42) Vatamanu, J.; Kusalik, P. G. Observation of two-step nucleation in methane hydrates. *Phys. Chem. Chem. Phys.* **2010**, *12* (45), 15065−15072.
(43) Matsumoto, M. Four-Body Cooperativity in Hydrophonic Association of Methane. *J. Phys. Chem. Lett.* **2010**, *1* (10), 1552−1556.
(44) Jacobson, L. C.; Hujo, W.; Molinero, V. Amorphous Precursors in the Nucleation of Clathrate Hydrates. *J. Am. Chem. Soc.* **2010**, *132* (33), 11806−11811.
(45) Li, Y.; Wu, N.; He, C.; Sun, Z.; Zhang, Z.; Hao, X.; Chen, Q.; Bu, Q.; Liu, C.; Sun, J. Nucleation probability and memory effect of methane-propane mixed gas hydrate. *Fuel* **2021**, *291*, 120103.
(46) Yagasaki, T.; Matsumoto, M.; Andoh, Y.; Okazaki, S.; Tanaka, H. Effect of Bubble Formation on the Dissociation of Methane Hydrate in Water: A Molecular Dynamics Study. *J. Phys. Chem. B* **2014**, *118* (7), 1900−1906.
(47) Yagasaki, T.; Matsumoto, M.; Andoh, Y.; Okazaki, S.; Tanaka, H. Dissociation of Methane Hydrate in Aqueous NaCl Solutions. *J. Phys. Chem. B* **2014**, *118* (40), 11797−11804.
(48) Ji, H.; Chen, D.; Zhao, C.; Wu, G. Molecular Dynamics Simulation of Methane Hydrate Formation and Dissociation in the Clay Pores with Fatty Acids. *J. Phys. Chem. C* **2018**, *122* (2), 1318−1325.
(49) Liang, S.; Liang, D.; Wu, N.; Yi, L.; Hu, G. Molecular Mechanisms of Gas Diffusion in CO2 Hydrates. *J. Phys. Chem. C* **2016**, *120* (30), 16298−16304.
(50) Liang, S.; Yi, L.; Liang, D. Molecular Insights into the Homogeneous Melting of Methane Hydrates. *J. Phys. Chem. C* **2014**, *118* (49), 28542−28547.
(51) Rosenbaum, E. J.; English, N. J.; Johnson, J. K.; Shaw, D. W.; Warzinski, R. P. Thermal conductivity of methane hydrate from experiment and molecular simulation. *J. Phys. Chem. B* **2007**, *111* (46), 13194−13205.
(52) Miguez, J. M.; Conde, M. M.; Torre, J. P.; Blas, F. J.; Pineiro, M. M.; Vega, C. Molecular dynamics simulation of CO2 hydrates: Prediction of three phase coexistence line. *J. Chem. Phys.* **2015**, *142* (12), 124505.
(53) Zhang, Z.; Guo, G.-J.; Wu, N.; Kusalik, P. G. Molecular Insights into Guest and Composition Dependence of Mixed Hydrate Nucleation. *J. Phys. Chem. C* **2020**, *124* (45), 25078−25086.
(54) Michalis, V. K.; Costandy, J.; Tsimpanogiannis, I. N.; Stubos, A. K.; Economou, I. G. Prediction of the phase equilibria of methane hydrates using the direct phase coexistence methodology. *J. Chem. Phys.* **2015**, *142* (4), 044501.
(55) Michalis, V. K.; Tsimpanogiannis, I. N.; Stubos, A. K.; Economou, I. G. Direct phase coexistence molecular dynamics study of the phase equilibria of the ternary methane−carbon dioxide−water hydrate system. *Phys. Chem. Chem. Phys.* **2016**, *18* (34), 23538−23548.
(56) Yuhara, D.; Brumby, P. E.; Wu, D. T.; Sum, A. K.; Yasuoka, K. Analysis of three-phase equilibrium conditions for methane hydrate by isometric-isothermal molecular dynamics simulation. *J. Chem. Phys.* **2018**, *148* (18), 184501.
(57) Poling, B. E.; Prausnitz, J. M.; O'connell, J. P. *Properties of gases and liquids*, McGraw-Hill Education 2001.
(58) Zhang, Z.; Kusalik, P. G.; Guo, G.-J. Bridging solution properties to gas hydrate nucleation through guest dynamics. *Phys. Chem. Chem. Phys.* **2018**, *20* (38), 24535−24538.
(59) Abascal, J. L. F.; Sanz, E.; Fernandez, R. G.; Vega, C. A potential model for the study of ices and amorphous water: TIP4P/Ice. *J. Chem. Phys.* **2005**, *122* (23), 234511.
(60) Ryckaert, J. P.; Ciccotti, G.; Berendsen, H. J. C. Numerical integration of the cartesian equations of motion of a system with constraints: molecular dynamics of n-alkanes. *J. Comput. Phys.* **1977**, *23* (3), 327−341.
(61) Hess, B.; Bekker, H.; Berendsen, H. J. C.; Fraaije, J. LINCS: A linear constraint solver for molecular simulations. *J. Comput. Chem.* **1997**, *18* (12), 1463−1472.
(62) Essmann, U.; Perera, L.; Berkowitz, M. L.; Darden, T.; Lee, H.; Pedersen, L. G. A smooth particle mesh Ewald method. *J. Chem. Phys.* **1995**, *103* (19), 8577−8593.
(63) Hoover, W. G. Canonical dynamics: Equilibrium phase-space distributions. *Phys. Rev. A* **1985**, *31* (3), 1695−1697.
(64) Parrinello, M.; Rahman, A. Polymorphic transitions in single crystals: A new molecular dynamics method M. Parrinello; A. Rahman. *J. Appl. Phys.* **1981**, *52* (12), 7182−7190.
(65) Abraham, M. J.; Murtola, T.; Schulz, R.; Pall, S.; Smith, J. C.; Hess, B.; Lindahl, E. GROMACS: high performance molecular simulations through multi-level parallelism from laptops to supercomputers. *SoftwareX* **2015**, *1−2*, 19−25.
(66) Szilard, P.; Abraham, M. J.; Kutzner, C.; Hess, B.; Lindahl, E. Tackling Exascale Software Challenges in Molecular Dynamics Simulations with GROMACS arXiv. *arXiv* **2015**, *27*, 27.
(67) Humphrey, W.; Dalke, A.; Schulten, K. VMD: Visual molecular dynamics. *J. Mol. Graphics Modell.* **1996**, *14* (1), 33−38.

https://doi.org/10.1021/acsomega.4c00108
ACS Omega 2024, 9, 25822−25831

(68) Zhang, Z.; Kusalik, P. G.; Guo, G.-J. Might a 2,2-Dimethylbutane Molecule Serve as a Site to Promote Gas Hydrate Nucleation? *J. Phys. Chem. C* **2019**, *123* (33), 20579−20586.
(69) He, Z.; Linga, P.; Jiang, J. What are the key factors governing the nucleation of CO2 hydrate? *Phys. Chem. Chem. Phys.* **2017**, *19* (24), 15657−15661.
(70) Walsh, M. R.; Rainey, J. D.; Lafond, P. G.; Park, D.-H.; Beckham, G. T.; Jones, M. D.; Lee, K.-H.; Koh, C. A.; Sloan, E. D.; Wu, D. T.; et al. The cages, dynamics, and structuring of incipient methane clathrate hydrates. *Phys. Chem. Chem. Phys.* **2011**, *13* (44), 19951−19959.
(71) Walsh, M. R.; Beckham, G. T.; Koh, C. A.; Sloan, E. D.; Wu, D. T.; Sum, A. K. Methane Hydrate Nucleation Rates from Molecular Dynamics Simulations: Effects of Aqueous Methane Concentration, Interfacial Curvature, and System Size. *J. Phys. Chem. C* **2011**, *115* (43), 21241−21248.
(72) Pang, J.; Liang, Y.; Masuda, Y.; Takeya, S. Structural Transition of the Methane-Ethane Mixture Hydrate in a Hydrate/Water/Hydrocarbon Three-Phase Coexistence System: Effect of Gas Concentration. *ACS Sustainable Chem. Eng.* **2020**, *8* (45), 16924−16937.
(73) Li, S.; Lv, R.; Yan, Z.; Huang, F.; Zhang, X.; Chen, G.-J.; Yue, T. Design of Alanine-Rich Short Peptides as a Green Alternative of Gas Hydrate Inhibitors: Dual Methyl Group Docking for Efficient Adsorption on the Surface of Gas Hydrates. *ACS Sustainable Chem. Eng.* **2020**, *8* (10), 4256−4266.
(74) Liang, S.; Rozmanov, D.; Kusalik, P. G. Crystal growth simulations of methane hydrates in the presence of silica surfaces. *Phys. Chem. Chem. Phys.* **2011**, *13* (44), 19856−19864.
(75) Yi, L.; Zhou, X.; He, Y.; Cai, Z.; Zhao, L.; Zhang, W.; Shao, Y. Molecular Dynamics Simulation Study on the Growth of Structure II Nitrogen Hydrate. *J. Phys. Chem. B* **2019**, *123* (43), 9180−9186.
(76) Zhang, Z.; Kusalik, P. G.; Guo, G.-J. Molecular insight into the growth of hydrogen and methane binary hydrates. *J. Phys. Chem. C* **2018**, *122* (14), 7771−7778.
(77) Lu, Y.; Wang, H.; Li, Q.; Lv, X.; Ge, Y.; Zhang, L.; Zhao, J.; Yang, L.; Song, Y. CO2 storage behavior via forming hydrate from N2/CO2 gas mixtures in the presence of initial SI CO2 hydrate seeds. *Chem. Eng. J.* **2022**, *450*, 138001.
(78) Chen, Y.; Chen, C.; Sum, A. K. Propane and Water: The Cooperativity of Unlikely Molecules to Form Clathrate Structures. *J. Phys. Chem. B* **2020**, *124* (22), 4661−4671.
(79) Chen, Y.; Chen, C.; Sum, A. K. Molecular Resolution into the Nucleation and Crystal Growth of Clathrate Hydrates Formed from Methane and Propane Mixtures. *Cryst. Growth Des.* **2021**, *21* (2), 960−973.
(80) Lu, Y.; Yang, L.; Kuang, Y.; Song, Y.; Zhao, J.; Sum, A. K. Molecular simulations on the stability and dynamics of bulk nanobubbles in aqueous environments. *Phys. Chem. Chem. Phys.* **2021**, *23*, 27533−27542.
(81) Liang, H.; Yang, L.; Song, Y.; Zhao, J. New Approach for Determining the Reaction Rate Constant of Hydrate Formation via X-ray Computed Tomography. *J. Phys. Chem. C* **2021**, *125* (1), 42−48.
(82) Arjun, A.; Bolhuis, P. G. Molecular Understanding of Homogeneous Nucleation of CO2 Hydrates Using Transition Path Sampling. *J. Phys. Chem. B* **2021**, *125* (1), 338−349.

https://doi.org/10.1021/acsomega.4c00108
ACS Omega 2024, 9, 25822−25831